NATIONAL TECHNICAL UNIVERSITY OF ATHENS
SCHOOL OF CHEMICAL ENGINEERING
DEPARTMENT OF PROCESS ANALYSIS & PLANT DESIGN

Multiscale analysis of chemical vapor deposition of copper

This research is co-financed by Greece and the European Union (European Social Fund- ESF) through the Operational Programme «Human Resources Development, Education and Lifelong Learning» in the context of the project "Reinforcement of Postdoctoral Researchers - 2nd Cycle" (MIS-5033021), implemented by the State Scholarships Foundation (IKY).

Nikolaos Cheimarios

Supervisor

Andreas G. Boudouvis

Athens, 23/11/2021

Ευρωπαϊκή Ένωση
European Social Fund

Operational Programme
Human Resources Development,
Education and Lifelong Learning
Co-financed by Greece and the European Union

ΕΣΠΑ 2014-2020
ανάπτυξη - εργασία - αλληλεγγύη

Contents

1 Introduction

Chemical Vapor Deposition CVD is a widely used process for producing thin solid films and, nanoscale structures from gaseous reactants. Its applications range from coatings for wear and corrosion resistance, high temperature protection and erosion protection, to semiconductors and related devices (integrated circuits, sensors and optoelectronic devices), optical fibers for telecommunications, composites, powders and nanomachines, nanostructures, and nanowires[1]. Compared to physical deposition techniques (PVD), such as sputtering, sublimation, evaporation and other chemical based deposition techniques such as atomic layer deposition (ALD), CVD has the ability to produce a large variety of films and coatings of metals, semiconductors, and inorganic as well as organic compounds, possessing reproducible and controllable properties. The latter include film composition, uniformity, surface morphology, purity and uniform thickness on highly irregularly shaped surfaces. These properties vary with the application and material and they strongly depend on the usage of the fabricated device.

CVD is performed in specially designed reactors, the CVD reactors, equipped with the wafers or substrates, where the film is deposited through surface reactions. The gaseous reactants, including the precursor i.e., the compound that carries the chemical species to be deposited, enter the CVD reactor and are guided by agas, the carrier gas, to the wafer where the surface reactions and the deposition of the film occurs.

CVD is a multiscale process: From the macro (or bulk or gas phase) of the CVD reactor – of the order of some cm or even m – to the micro-scale of a predefined topography on the wafer's surface – of the order of μm - or the nano-scale of the growing surface of the film which is of the order of nm or Å different processes are performed. Depending on the level of detail, dictated by the underlying theoretical or technological question, someone can study a CVD process in one of these scales or perform multiscale analysis.

The present study focuses on the multiscale modeling of Copper (Cu) CVD from a novel precursor, namely from copper(I) N,N′-di-isopropylacetamidinate $[Cu(iPr–Me–amd)]_2$ or $[Cu(amd)]_2$ where amd = $CH(CH_3)_2NC(CH_3)NCH(CH_3)_2$[2]. Cu tends to replace Al in the interconnection of modern integrated circuits because of improved properties against Al. Specifically, Cu shows lower resistance, twice the thermal conductivity, 100 times greater resistance to electromigration which eventually can lead to material failure[3]–[5]. The deposition of Cu is yet challenging, especially in industrial scale since robust methods for depositing Cu films

are still unknown or the existing methods are insufficient due to lack of appropriate materials. $[Cu(amd)]_2$ was proposed by [2]as a Cu precursor because if its properties against other Cu precursors such as low deposition temperatures, it is stable in the presence of other substances containing oxygen of halogens and high thickness uniformity[6].

In our previous work[6], based on the experimental work of[7],we proposed a deposition mechanism depending on the thermal region of deposition. In low temperatures regions ($T < 506$ K) an Arrhenius type kinetics was proposed and for higher temperatures ($T > 506$ K) a Langmuir–Hinshelwood (LH) mechanism. The different reaction kinetics were proposed to capture the decrement of the deposition rate as the temperature increased. Similar behaviors have been observed previously for other systems, e.g. Al systems, but this decrement was attributed to the existence of volumetric reactions – i.e. reactions that perform in the bulk phase of the CVD reactor and not in the substrate –which result on the depletion of the precursor. The experimental work of[7], suggested that in the case of $[Cu(amd)]_2$ there is only a single surface reaction taking place in the substrate[see Eq. (S2.1)]and no volumetric reactions up until 573 K. For that, based on previous works[8], [9],for the deposition of Cu from another precursor, namely $Cu(hfac)_2$, we proposed a LH reaction mechanism which takes into account inhibition effects from amd. Very recently, Spencer et al. [10]proposed a detailed model which assumes volumetric reactions in the entire temperature deposition spectrum. Their computational are in an excellent agreement with the experimental data. Nevertheless, their work did not cover multiple scales and for that could not explicitly take into account amd inhibitions effects.

In this work we explore if amd can act as an inhibitor and reduce the deposition rate in high temperatures in a CVD multiscale context. In order to explore the inhibition effects by amd we link the computations in the macro-scale of a CVD reactor with a kinetic Monte Carlo model which takes into account explicitly the inhibition effects by amd. The macro-scale computations provide the mass fluxes of the different reactants reaching the substrate surface which are then used by the KMC software to perform the various processes that mimic the growth of Cu. Furthermore, we performed nonlinear computations in the macro-scale model of the CVD reactor in order to investigate if the transport phenomena can affect the deposition rate at high temperatures and we expand our previous nonlinear computations [11] to investigate the effect of the self-sustained periodic solutions to the deposition rate and films thickness non-uniformity.

2. Modelling the macro-scale of the CVD reactor

Due to the importance of the CVD processes in academia and industry, macro-scale CVD reactor models are well established through a series of work during the past four decades[12]–[18]. These models are based on the conservation laws of mass, momentum, energy, and species mass fraction and are described by partial differential equations[1].

2.1 Governing equations

At steady state and in vector notation the aforementioned set of equations is,

a) Continuity equation

$$\nabla \cdot (\rho \boldsymbol{u}) = 0 \tag{2.1}$$

where ρ is the density of the gas mixture and **u** the velocity.

b) Momentum equation

$$\begin{aligned} \nabla \cdot (\rho \boldsymbol{u}\boldsymbol{u}) = -\nabla P + \nabla \\ \cdot \left[\mu(\nabla \boldsymbol{u} + \nabla \boldsymbol{u}^T)\right. \\ \left. - \mu \frac{2}{3}(\nabla \cdot \boldsymbol{u})\boldsymbol{I}\right] + \rho \boldsymbol{g} \end{aligned} \tag{2.2}$$

whereP is the pressure, μ the viscosity, **I** the unit tensor, and **g** is the gravity acceleration.

c) Energy equation

$$\begin{aligned} C_p \nabla \cdot (\rho \boldsymbol{u} T) = \nabla \cdot (\lambda \nabla T) \\ - \sum_{i=1}^{N_{species}} \boldsymbol{j}_i \cdot \frac{\nabla H_i}{M_i} \\ - \sum_{i=1}^{N_{species}} \sum_{k=1}^{N_r} H_i \gamma_{ik} r_k^g \end{aligned} \tag{2.3}$$

where C_p is the specific heat of the gas mixture, T the temperature, λ the thermal conductivity, $\mathbf{j}_i$ the diffusive mass flux of species i, H_i the enthalpy of formation of species i, M_i the molecular

weight of species *i*, γ_{ik} the stoichiometric coefficient of species *i* in reaction *k*, $N_{species}$ the number of species in the gas phase, N_r the number of volumetric reactions, and r_k^g is the molar rate of volumetric reaction *k*.

d) Species transport equation

$$\nabla \cdot (\rho \boldsymbol{u} y_i) = -\nabla \cdot \boldsymbol{j}_i + M_i \sum_{k=1}^{N_r} \gamma_{ik} r_k^g, i = 1, \dots, N-1 \tag{2.4}$$

where y_i is the mass fraction of species *i*. The aforementioned system of equations closes with the ideal gas law. The latter equations are discretized and solved with both CFD software Fluent [19] and Comsol [20]. Fluent model is used for the multiscale modeling while the Comsol model for the nonlinear analysis (see details in Section 5).

2.2 Reactor geometry, species mixture properties& boundary conditions

The macro-scale model is a 3D stagnation flow, cold wall, CVD reactor described in detail in previous works[6], [10], [21], [22](see Fig. 2.1a,b). A 3D model is necessary to describe the phenomena inside the reactor because of the showerhead, which is used to homogenize the flow above the substrate, consists of 1450 holes of 0.76 mm diameter (see Fig. 2.1b and d). The thickness of the plate is 3 mm. A mesh of 1.232.468 cells comes out to be an appropriate one bases on mesh independent study. Due to the size of the resulting computational problem, parallel processing in computer clusters is indispensable. The CPU time and memory required for the solution of 3D problem are ~4 h and 2 GB, respectively in Fluent software.

For the case of Cu CVD, the properties of the individual species and of the mixture are computed as in [6]. The Lennard-Jones (LJ) parameters, namely σ and ε, are the parameters of the LJ potential and are needed for the estimation of the properties in the gas phase of the CVD reactor. σ is the measure of the size of the molecules and ε/k is a measure of how strongly the molecules attract each other. For the unknown species, namely $[Cu(amd)]_2$ and H(amd), their

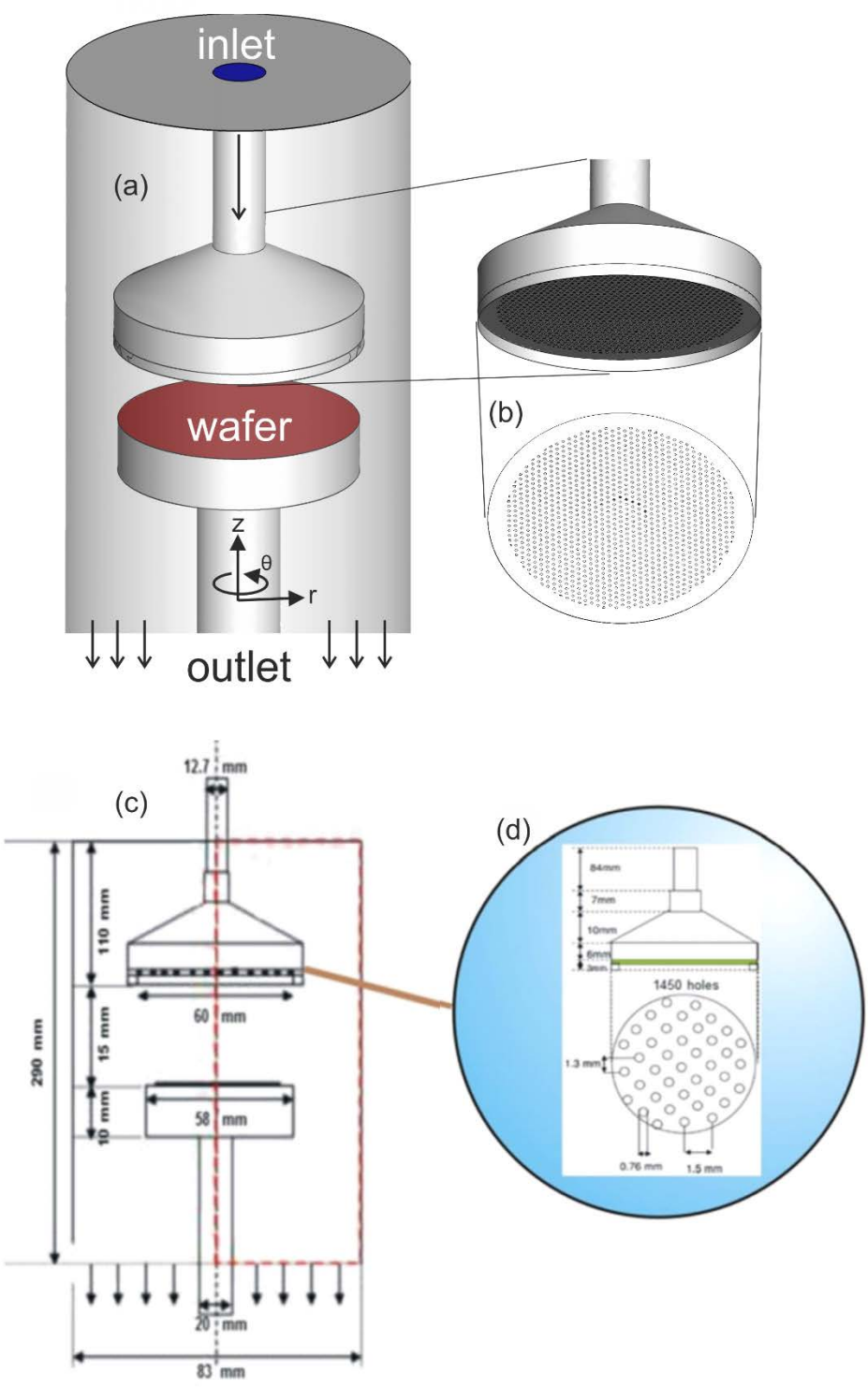

Figure 2.1 (a) The bulk phase of the CVD reactor (b) Details of the showerhead which is used to homogenize the flow above the wafer (c) Dimensions of the CVD reactor and (d) dimensions of showerhead.

values are calculated with group contribution methods and for $[Cu(amd)]_2$ are: σ = 10.8525 Å and ε/k = 423.2 K and for H(amd): σ = 9.4874 Å and ε/k = 534.8 K.

Concerning the boundary conditions, for the velocity: at the inlet of the reactor a constant mass inflow rate of 7.473×10^{-6} kg/s is imposed. No-slip condition is imposed at all the walls of the reactor. At the outlet, a standard outflow boundary condition is used. For the species: the mass fractions of the species entering the reactor are $y_{[Cu(amd)]_2} = 0.001016$, $y_{H_2} = 0.004107$ and $y_{N_2} = 0.2556$; the rest is Ar. The flux of all species at the reactor walls is zero with an exception on the substrate where the surface reactions (deposition) take place. An overall mass balance correction is imposed at the outlet. The operating pressure of the reactor is 1333 Pa. The wafer temperature, T_w, varies as 473 K, 493 K, 513 K, 533 K, 553 K, 573 K, 593 K and 623 K, according to the available experimental data.

2.3 Surface reaction kinetics in the macro-scale model

Based on the experimental work of [7],we assume only a single surface reaction which leads to the deposition of Cu, namely,

$$[Cu(amd)]_{2(g)} + H_{2(g)} \rightarrow 2Cu_{(s)} + 2H(amd)_{(g)} \quad \text{(S2.1)}$$

Two reaction kinetics expressions are used; for T_w= 473 K to 513 K an Arrhenius expression is used and from 533 K to 623 K a Langmuir-Hinshelwood (LH) expression. The Arrhenius expression reads,

$$r_A = k_A \exp\left(-\frac{E_1}{RT}\right) C_{[Cu(amd)]_2} C_{H_2} \quad (2.5)$$

where k_A= 1.33 10^{10} KJ/(m^2 mol) and E_1= 66 KJ/mol and the LH reads,

$$r_{LH} = \frac{k_a k_d C_{[Cu(amd)]_2} C_{H_2}}{\left(2k_a C_{[Cu(amd)]_2} + k_c C_{H(amd)}\right) + k_d C_{H_2}} \quad (2.6)$$

Eq. 2.6 takes implicitly into account inhibition effects from H(amd). The parameters $k_d = r_A$, $k_a = 0.07\ \left[\frac{m}{s}\right]$and $k_c = 0.01\ \left[\frac{m}{s}\right]$ are fitted to the experimental data. None of the above kinetics is valid on the entire spectrum of T_w; the Arrhenius type is valid on low and the LH on high temperatures.

3. Monte Carlo &Kinetic Monte Carlo methods in deposition processes

Monte Carlo (MC) and kinetic Monte Carlo (kMC) are widely used methods in many fields of science and engineering: From materials science and polymers properties [23], astrophysics and black holes mergers [24] to computational geometry and volume approximation [25]. Their popularity in materials science stems from their inherit ability to simulate the molecular level of materials seamlessly. In MC/kMC, the particles (molecules, atoms, beads) move stochastically according to specific rules (events/processes), transferring the system randomly over the phase-space and approximating the mean values of various properties. In contrast to other molecular methods such as molecular dynamics (MD), the system in MC cannot easily be trapped in local energy minima and even if it is trapped, it can be "kicked out" to other states by incorporating sophisticated events. Furthermore, kMC filters out vibrational movements, allowing it to run over much larger spatial and time scales than MD. Especially in film growth, snapshots of MC/kMC simulation can be directly related and compared to scanning tunneling microscopy images.MC/kMC have notable applications in the study of film deposition processes—probably the most important in the fabrication of semiconductor devices.

During any deposition process the material is deposited upon a surface either by physical or chemical processes. In physical processes, the material is injected as a gas and sticks (adsorbs) on the deposition surface with a probability (or rate). PVD, which encompasses sputtering and evaporation, belongs to this category of deposition processes. In chemical processes, the material is grown on the deposition surface through surface reactions.

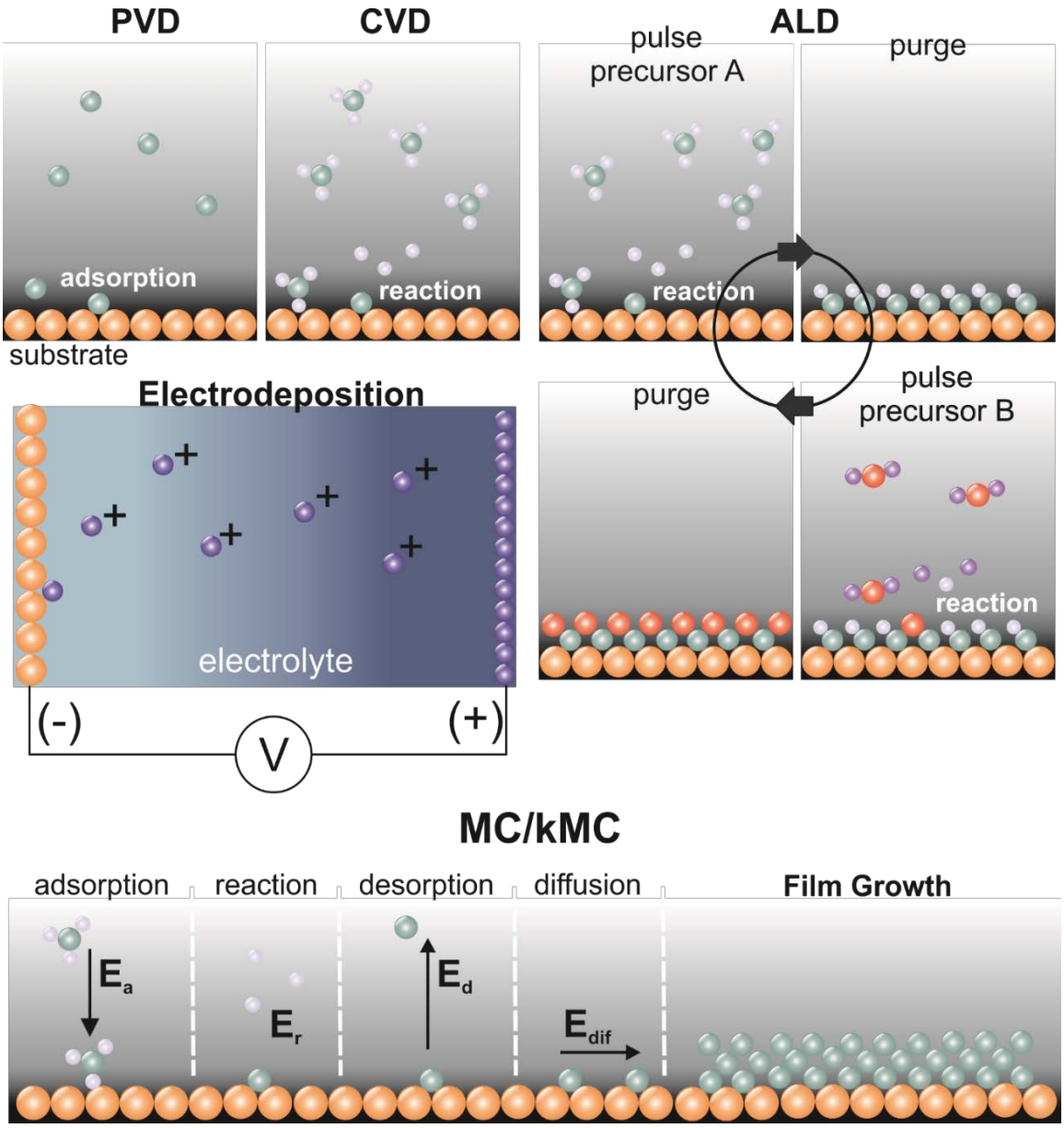

Figure 3.1 Schematic representation at the molecular level of the basic principles in deposition processes. In PVD, particles are adsorbed in the substrate. In CVD, particles (here an arbitrary molecule is shown) react on the substrate surface to grow the film. In ALD, multiple precursors (here A & B) are injected into the reactor though pulses in a cyclic way of pulses-purges and grow the film through self-limiting surface reactions. In electrodeposition, the voltage (V) is applied causing the particles from the cathode to move to the anode through an electrolyte where the film is grown through adsorption or surface reactions. In MC/kMC methods, an activation energy is assigned to each event. In MC, if the event leads the system to a smaller energy, it is accepted unconditionally. If not, it is selected with a probability according to Eq. 3.2. In kMC, an event is selected from a predefined rate catalog containing all possible rates and performed unconditionally. Then the system evolves in time according to Eq.3.8. The four basic events – adsorption, reaction, desorption and diffusion- whose combination can describe a deposition process, with their activation energies, E_a, E_r, E_d and E_{dif} are shown.

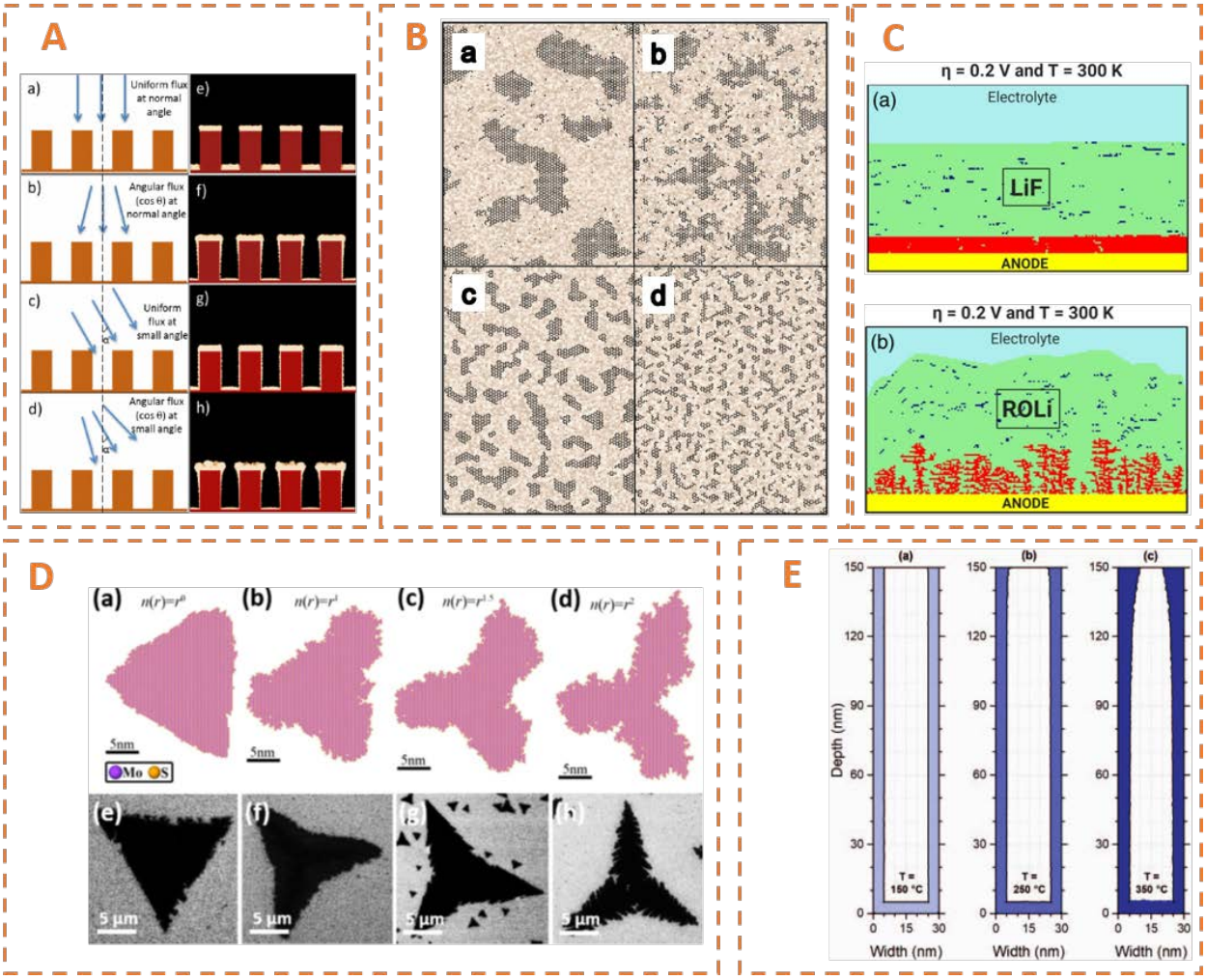

Figure 3.2 A. PVD of Ag core/shell on In_2S_3 nanorods: MC results for four different conditions: (a & e) Uniform incident flux, α = 0º (α is the angle between the incoming flux and the surface normal to the substrate), (b & f) angular flux ~cos(θ) with α = 0º, (c & g) uniform flux with α = 30º and (d & h) angular flux ~ cos(θ) with α = 30º (reprinted with permission from ref. [26]) **B.** Graphene CVD: MC results for varying strength of surface roughness parameter ξ and mobility parameter T_s for (a) $\xi = 1.2$, $T_s = \infty$ (b) $\xi = 1.5$, $T_s = \infty$ (c), $\xi = 1.5$, $T_s = 0$ and (d) $\xi = 1.2$, $T_s = 0$. The color represents roughness (reprinted with permission from ref. [27]). **C.** Electrodeposition in Li metal anode: kMC results for (a) uniform Li deposition in LiF electrolyte, (b) dendrite growth in ROLi electrolyte. The red particles represent the Li metal which is being deposited, and the dark-blue particles represent the Li+ ions which are diffusing. The process conditions (η - activation overpotential and T – temperature) are also shown (reprinted with permission from ref. [28]). **D.** MoS_2 CVD: kMC results for the morphology of MoS_2 as a function of the Mo density gradient, $n(r) - r$ distance from Mo source (a) no Mo density gradient, $n(r) = r^0$ (b-d) $n(r) = r^1$, $n(r) = r^{1.5}$, and $n(r) = r^2$ (e–h) corresponding SEM images (reprinted with permission from ref. [29]). **E.** SiN_x ALD: Thickness profile in a micro-structure with aspect ratio equal to 5 for parasitic CVD (no-ALD) reactions at different T_w (a) 150 ºC, (b) 250 ºC and (c) 350 ºC, determined by kMC computations (reprinted with permission from ref. [30]).

Examples of chemical deposition processes are CVD, ALD and electrochemical deposition. In the context of MC/kMC methods the different processes are shown schematically in Fig. 3.1.

Concerning the recent works of MC and kMC on deposition processes, most PVD computational works deal with the growth of nanorods[26], [27], [31]–[33] while in CVD, most works examine the growth of graphene[29], [34]–[40], followed by 2D materials and namely Transition metal dichalcogenides (TMDs - MoS_2, WSe_2 and WS_2)[41]–[46]. kMC models have also been developed for the deposition of diamond [47], GaAs [48] and AlN [49]film, plasma enhanced a-Si:H CVD [50], hybrid MD/kMC [51] and for growth in extereme pressure conditions [52]. Concerning ALD, most works deal with the study of step coverage inside micro-/nano-features,[30], [53]–[56]. In the context of electrodeposition, most work perform MC/kMC to study the properties of Li anodes metal batteries[57], [58]. Representative results from the MC/kMC models applied in recent works for deposition processes are shown in Fig. 3.2.

3.1 The kMC method

In MC and kMC algorithms, sequential events are performed stochastically. MC solves the steady state Master Equation (ME) and kMC the transient one. The transient ME reads,

$$\frac{\partial p_j(t)}{\partial t} = \sum_{i \neq j} p_i\,(t) T_{ij} - \sum_{i \neq j} p_j(t)\, T_{ji} \tag{3.1}$$

where $p_{j(i)}$is the probability of the system to be found in state j (i) at time t. T_{ij} and T_{ji} denote the transition rate or transition probability from state i to j and vice versa. Each event occurs at a certain probability/rate to form a Markov chain[59]. To generate the Markov chain the desired probability distribution $p_{i(j)}$ must obey the detailed balanced condition,

$$p_i T_{ij} = p_j T_{ji} \tag{3.2}$$

$p_{i(j)}$are Boltzmann distributions,

$$p_{i(j)} = exp\left(-\frac{E_{i(j)}}{k_b T}\right) \tag{3.3}$$

where $E_{i(j)}$ is the energy of the system in state *i(j)*. [60] proposed that,

$$T_{ij} = \begin{cases} 1, & \text{if } \Delta E \leq 0 \\ exp\left(-\frac{\Delta E}{k_b T}\right), & \text{if } \Delta E > 0 \end{cases} \tag{3.4}$$

so that the system will unconditionally move from state *i* to *j* if $\Delta E<0$ and with a probability $exp\left(-\frac{\Delta E}{k_b T}\right)$ if $\Delta E > 0$, where $\Delta E = E_j - E_i$. Practically, a random number ξ is chosen between (0,1] and if $\xi < exp(-\Delta E/k_b T)$,the system moves to the state *j*, otherwise the move is rejected. In this way, different states of the system are generated and the thermodynamic average of a quantity q_i reads,

$$\langle q \rangle = \frac{\sum_i q_i p_i}{\sum_i p_i} \tag{3.5}$$

kMC method solves Eq. 1. The most popular algorithm proposed by Bortz et al. [61]is termed as the *N*-fold method. In the *N*-fold method random transitions from *i* to *j* are performed unconditionally based on the transition rates, so that more likely transitions are selected more often. Every transition event *i* is assigned a rate which reads,

$$r_i = v_i \, exp\left(-\frac{E_i}{k_b T}\right) \tag{3.6}$$

where v_i is a frequency prefactor, E_i is the energy barrier and *T* is the temperature. Practically, the simulation starts by defining all rates (rate catalog) r_i of all possible processes that describe the physical problem. The total rate, $R = \sum_i r_i$, is first computed and then a process *n* is randomly chosen according to,

$$\sum_{i=1}^{n} \frac{r_i}{R} < \xi_1 < \sum_{i=1}^{n+1} \frac{r_i}{R} \tag{3.7}$$

where ξ_1 is randomly chosen in (0,1) and a single event is performed. The time advances as $t = t + \Delta t$ with Δt being,

$$\Delta t = -\frac{ln\,\xi_2}{R} \tag{3.8}$$

where ξ_2 is an additional random number chosen in (0,1). R is recalculated based on the new system state. The algorithm stops when the desired time interval is reached.

kMC rates must obey also the detailed balance condition (Eq. 3.2), even if the system is not in equilibrium, to ensure the dynamic evolution will correspond to a physical system [62]. kMC rates depend on both the particle and the lattice type that participate in the process and can be calculated via Transition State and Harmonic Transition State Theories (TST – HTST [62]), Density Functional Theory (DFT) and *ab initio* methods (e.g. [39], [41], [43], [44]).

Focusing on the deposition processes, the notion of lattice is of great importance. The lattice represents the deposition surface and is composed of sites upon which all events occur, simplifying the construction of the rate catalog. Depending on how the lattice is represented, the atomistic information can either be presented in full detail (e.g. [63]) or in a coarse-grained way where microscopic neighboring sites are coalesced into coarse cells (e.g. [64], [65]). Off-lattice kMC [66] methods have also been proposed in atomistic representation where the rate catalog is computed "on the fly" in every step.

3.2 kMC model of Cu deposition from $[Cu(amd)]_2$

The reaction mechanism proposed in this work is based on the first principles computations of[67]. According to their work, the most energetically favorable process is the dissociation of $[Cu(amd)]_2$ onto the substrate and the occupation of four positions of the Cu surface: two by $Cu_2(amd)$ and two by amd (see Fig. 3.3). Thus, inhibitions effects are due to the adsorbed amd upon the surface. The H_2 above the substrate is in excess and according to our macro-scale computations, the mole fraction is ~1000 times more than $[Cu(amd)]_2$ (see Fig. 4.1), so we assume that H_2 does not limit the growth of Cu due to material inadequacy. As already stated, amd limits the growth rate because it blocks sites where $[Cu(amd)]_2$ can use to adsorb. The reaction of H_2

with amd leads to H(amd) which we assume that adsorbs instantly and releases potential sites for deposition. The latter mechanism is described as,

$$[Cu(amd)]_{2(g)} + 4* \rightarrow Cu_2(amd)\ (2*) + (amd)(2*) \quad \text{(S3.2)}$$

$$Cu_2(amd)(2*) + \frac{1}{2}H_{2(g)} \rightarrow 2* + 2Cu_{(s)} + H(amd)_{(g)} \quad \text{(S3.3)}$$

$$(amd)(2*) + \frac{1}{2}H_{2(g)} \rightarrow 2* + H(amd)_{(g)} \quad \text{(S3.4)}$$

Here Cu_2(amd) and amd are identical in terms of the reaction with H_2 since only the amd part reacts with H_2.

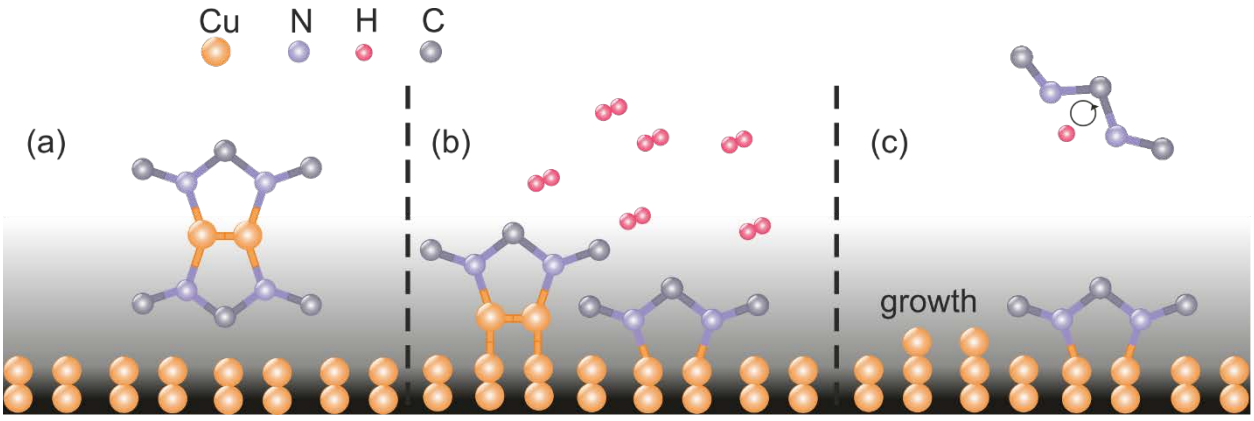

Figure 3.3 Schematic representation of the proposed reaction mechanism leading to the growth of Cu from $[Cu(amd)]_2$. (a) The $[Cu(amd)]_2$ molecule above the Cu surface. H on the $[Cu(amd)]_2$ molecule is not shown for simplicity. (b) Dissociation of $[Cu(amd)]_2$ molecule and inhibition effect from amd. $[Cu(amd)]_2$ cannot dissociate to sites occupied by amd. (c) Reaction with H_2, desorption of H(amd) and growth. The other amd still occupies two sites, preventing $[Cu(amd)]_2$ from dissociating to these sites.

The kMC model is based on Solid-On-Solid (SOS) approximation in a simple cubic lattice where $[Cu(amd)]_2$ dissociates upon four sites. We assume that the dissociation is performed instantly upon $[Cu(amd)]_2$ reaching the surface and thus the rate of the dissociation is the mass flux of $[Cu(amd)]_2$ reaching the substrate from the gas phase of the CVD reactor which reads[68],

$$r_1 = \frac{s_{[Cu(amd)]_2} < f_{[Cu(amd)]_2} > P_{op}}{N_a C_{tot} \sqrt{2\pi M_{[Cu(amd)]_2} kT}} \tag{3.9}$$

where $s_{[Cu(amd)]_2}$ and $< f_{[Cu(amd)]_2} >$ are the sticking coefficient and average over the wafer mole fraction of $[Cu(amd)]_2$ respectively, P_{op} the operation pressure of the reactor, N_a Avogadro's number, C_{tot} =2.0 10^{19} $[sites/m^2]$, the sites concentration on the surface of Cu, $M_{[Cu(amd)]_2}$ the molecular weight of $[Cu(amd)]_2$ and *k* Boltzmann's constant.

For the reaction of the adsorbed amd with H_2 the rate is given by,

$$r_2 = k_2 \exp\left(-\frac{n\, E_2}{R}\right) \tag{3.10}$$

$k_2 = 1.3\ 10^{13}\ [-]$, $E_2 = 8.965\ 10^4 \left[\frac{kj}{mol}\right]$and*n* is the number of nearest neighbors which are occupied by Cu (n = 2,3,4,5,6,7,8). That said, Eq. (3.10) takes into account the difficulty of the produced H(amd) to desorb and release the two sites for the dissociation of $[Cu(amd)]_2$. The pre-exponential factor and energy in Eq. (3.10) where fitted to the experimental data at 553 K from a single run and it was found that in order to capture the experimental data it should be a barrierless (athermal) process[69], [70]. H_2 is known to participate in barrierless processes as e.g. in the case of Si [71]–[73]. Still, such a claim must be investigated further via first principles, e.g. Density Functional Theory (DFT), computations[71] to better understand the mechanism and validate it.

3.3 The Apothesis software

There are many open-source software, based on the kMC method available online ([74]–[76]).However, these codes are primary for analyzing catalytic processes and not deposition, e.g.

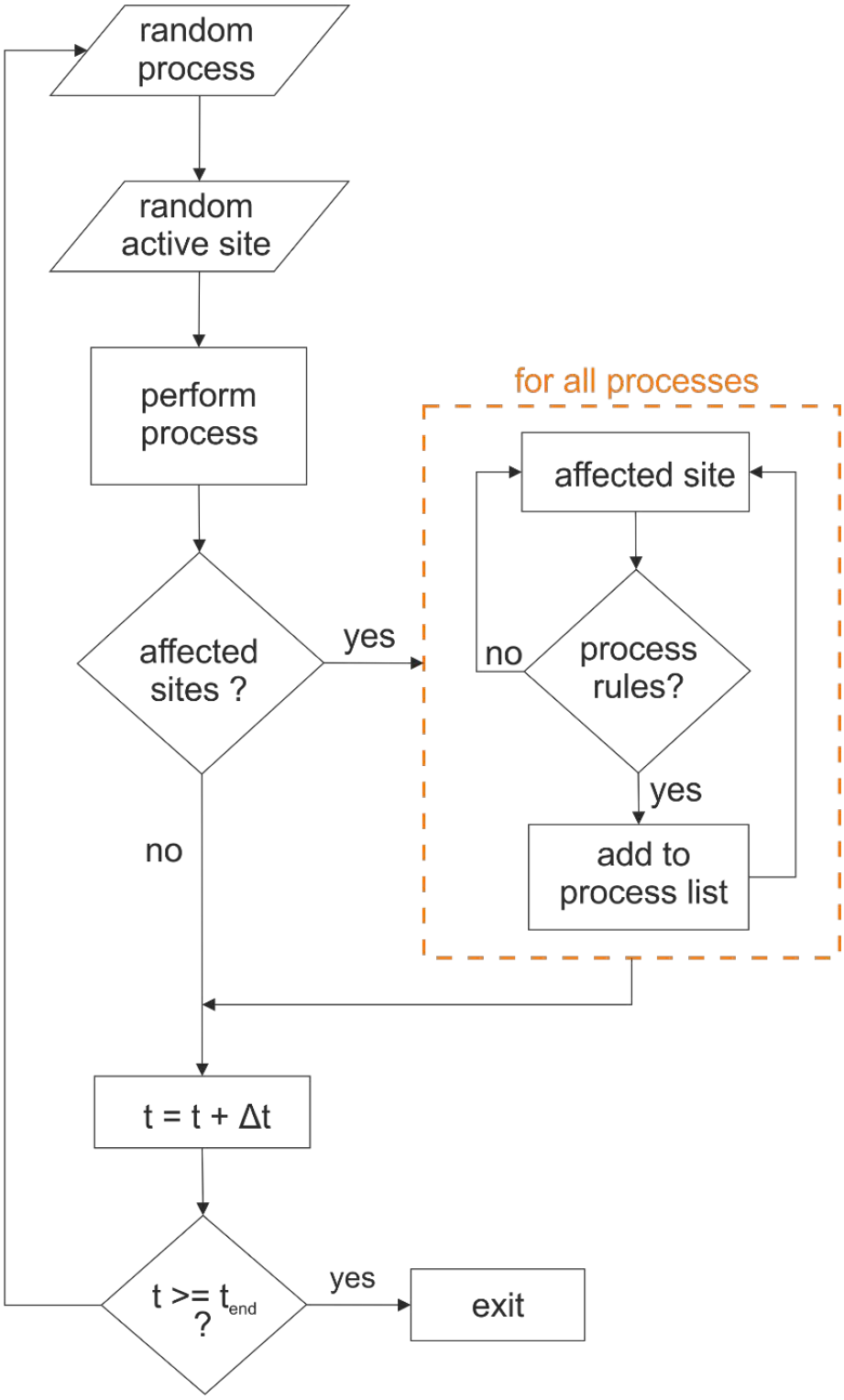

Figure 3.4 The computational "backbone" of Apothesis software. The algorithm starts by picking a random process and a random active site of this process. The process is performed and if it affects other sites a loop over all process is performed in order to update their lists according to their "rules" until all process lists are updated. After that the time is updated until the end time, t_{end} is reached.

they do not take into account the growth of the surface which is fundamental in deposition processes. Other software based on kMC[77], can be used only on the context of PVD since they cannot simulate chemical reactions. Other software with the same limitations have also been reviewed in [78].

In the context of this project, we developed the core of Apothesis. Apothesis is designed to be a generalized, psudo-3D kMC software for deposition processes based on the solid-on-solid approximation. Apothesis is written in C++ and an expansion in python is under design which will enable users to add any process without re-compiling the code.

The main components of Apothesis are the lattice and the processes. The lattice is a predefined number of positions, termed as sites, where the different processes can perform on. Depending on the material it can be simple cubic, Body Cubic Centered (BCC), Face Cubic Centered (FCC) etc. and depending on the orientation (001), (011), (111) etc. A process is an act on a site of the lattice. If a process can perform on a site, this site is termed as "activated" otherwise it is "blocked". An Apothesis process emulates a physical/chemical process e.g. the adoption of a species on an active site.

The sites of the lattice where a process can perform are kept on a list. The size of this list multiplied by the probability of the process is the process rate. In the course of a kMC simulation, each process list must be updated in order for the rates to be computed correctly. This make this part of the code crucial in terms of the validity of the software and in term of speed, since this is the most computational demanding part of kMC method in general. In order to generalize Apothesis, this part of the software should be very carefully designed and developed.

We tackled this issue by designing an abstract "Process" class which contains two primary functions, the "rules" and the "perform" functions. The "rules" function defines, computationally, when a process can be performed or not in a site and the "perform" is the process act on the lattice site. We take as an example the desorption of a particle of 4 nearest neighbors. The "rules" in this case would be to count the nearest neighbors of the site and if it is 4 then add it in its list. The "perform" would be to remove one particle (decrease site's height) and mark the sites that are affected which in this case are all 4 nearest neighbors. A loop is the performed to check, through the "rules", if the affected sites must be removed or added to any of the other process lists. In that way, the screening is performed in only a small number of sites, and not the entire lattice, reducing significantly the computational time. In this way, we construct a generalized framework where

every process can be described independently of the lattice and thus, producing a robust computational environment for kMC computations. The computational "backbone" of Apothesis can be seen schematically in Fig. 3.4. Apothesis is freely available in github: https://github.com/nixeimar/Apothesis under GPL license.

4. Multiscale modeling of CVD: Coupling/Linking reactor scale with kMC models

The first description for the need of linking a reactor scale model of a CVD reactor with kMC model is found in the work of Srolovitz et al.[79] for the CVD of diamond. In the same year, Vlachos [80], presented a model that coupled the reactor scale model of a chemical reactor with a KMC model in catalytic processes and then extended it for CVD processes[81]. Raimondeau and Vlachos[82] presented a coupling of the scales in a vertical CVD reactor while at the same period Masi et al.[83] presented a multiscale model for the CVD of Si from SiH_4. They linked the models at different scales by assuming that the growth rate is independent of the scale that it is computed i.e. the deposition rate is computed from the reactor scale model and for this value of the deposition rate, the species mass fractions on the wafer surface are transferred to the KMC model for computing the roughness of the growing film. The same assumption was made by Grujicic and Lai [84] for performing multiscale computations for diamond growth.

In 2001, Lam and Vlachos [187] showed the effect of the operating conditions of a CVD reactor on the roughness development and the growth rate of the film. Dollet [85] developed an integrated multiscale framework for the CVD of silicon carbites. In a series of works[86]–[89], Cavallotti and Barbato et al. developed multiscale computational frameworks which was mainly applied to Si deposition. Masi et al.[90] used a multiscale–multi-hierarchy approach, based on a succession of simplified models, to describe the deposition and the film morphology evolution during the epitaxial silicon carbide deposition in an industrial hot wall reactor.

More recently, we linked the different scales of Si and Al CVD[91], [92], by assuming that the computed growth rate is independent of the scale that it is computed from, as in the work by Masi et al.[83]. Aviziotis et al.[93], based on the same framework, performed multiscale computations for the Fe CVD. Wang et al.[94] performed coupled simulations with an MC model to predict the columnar growth of Cu nanorods for different operating pressures of a plasma reactor

and Christofides *et al.*[28], [95]–[99] conducted multiscale simulations of plasma assisted ALD processes, combining CFD and kMC models to characterize and control the process.

4.1 Linking the scales

The linking of the scales in this work is performed in the boundary condition for the species equations. We use the term linking since we send only information from the macro-scale model to the kMC model. Since, the use of the reaction kinetics in the macro-scale (see Eqs. 2.5 & 2.6) produces results that are in fair agreement with the experimental data, it offers a realistic approximation of the values of $< f_{[Cu(amd)]_2} >$. From $< f_{[Cu(amd)]_2} >$, the mass flux of [Cu(amd)]$_2$,$F_{[Cu(amd)]_2}$,can be computed as,

$$F_{[Cu(amd)]_2} = \frac{< f_{[Cu(amd)]_2} > P_{op}}{\sqrt{2\pi M_{[Cu(amd)]_2} kT}} \tag{4.1}$$

from which $s_{[Cu(amd)]_2}$isestimated as[100],

$$s_{[Cu(amd)]_2} = \frac{< r_A > (< r_{LH} >)}{F_{[Cu(amd)]_2}} \tag{4.2}$$

where $<r_A > (< r_{LH} >)$ are the average valuesover the substrate. The values of $s_{[Cu(amd)]_2}$ and $f_{[Cu(amd)]_2}$, needed in Eq. (2.7) of the kMC code,are computed from the macro-scale model and serve as the linking point of the different scales. Since no volumetric reactions are assumed and a good approximation of the kinetics in the macro-scale exist, the present multiscale scheme avoids time consuming computations as in the case of coupling, i.e. the by-directional transfer of information between the scales, which would require an iterative scheme [85], [88], [90], [101].

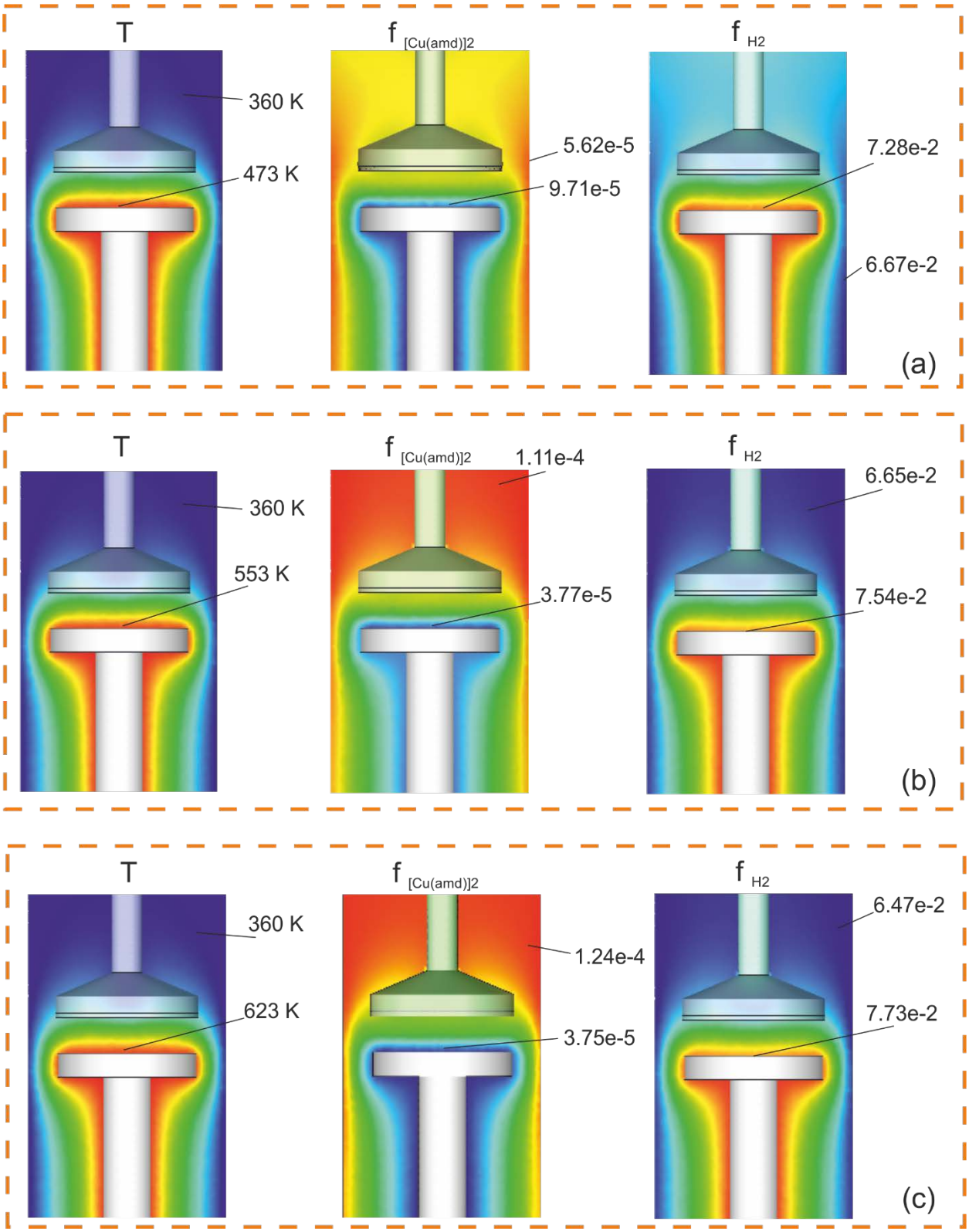

Figure 4.1 Temperature, $f_{[Cu(amd)]_2}$ and f_{H_2} distributions inside the CVD reactor for (a) T_w = 473 K, (b) T_w = 553 K and (c) T_w = 623 K. The maximum and minimum values are shown.

4.2 Results and discussion

Firstly, results from the computations in the macro-scale of the CVD reactor are presented. Three indicative T_w are selected based on the experimental data: 473 K where the lowest growth rate is observed, 553 K where the maximum growth rate is observed and 623 K where the maximum drop of the growth rate is observed as T_w increases. For these $T_w$the distributions of T, $f_{[Cu(amd)]_2}$and f_{H_2}inside the reactor are shown in Fig. 3.1. The$T$ distribution is almost identical for all T_w. Concerning the mole fractions distributions, $f_{[Cu(amd)]_2}$ in the cases of 533 K and 623 K is reduced compared to the 473 K case, which is expected since the reaction rate of $[Cu(amd)]_2$ is increased as T_w increases and more amount of $[Cu(amd)]_2$ is consumed. For the cases of 533 K and 623 K, $f_{[Cu(amd)]_2}$ is slightly reduced. Concerning f_{H_2}, there are no significant variations and can it can be considered as constant. It is noted that it is ~1,000 times more than $[Cu(amd)]_2$ which validates our assumption that the amount of H_2 is not the limited step for the calculation of the growth rate in S2-S4.

The growth rate computed by our macro-scale computations and the two different reaction kinetics expressions vs T_w is shown in Fig. 4.2. As stated in our previous work [6], the Arrhenius expression prediction is in excellent agreement with the experimental data in low T_w, but as T_w increases it fails to predict the growth rate. On the other hand, the LH fails in low T_w, but satisfactorily predicts the experimental data in high T_w. Thus, none is valid in the entire T_w spectrum. It must be noted that both expressions are empirical. Nevertheless, since their combination can predict the growth rate in fair agreement with the experimental data, it can be used to compute the necessary information for the kMC model as states in Section 2.2.

The average value of $< f_{[Cu(amd)]_2} >$used in the computation of $s_{[Cu(amd)]_2}$ from the macro-scale computations are shown in Table 4.1 for every T_w. As T_w increases, up until T_s 513 K, $< f_{[Cu(amd)]_2} >$ is decreased since the reaction rate increases. From 513 K until 573 K, $< f_{[Cu(amd)]_2} >$is practically constant and for 593 K and 623 K is slightly increased since the

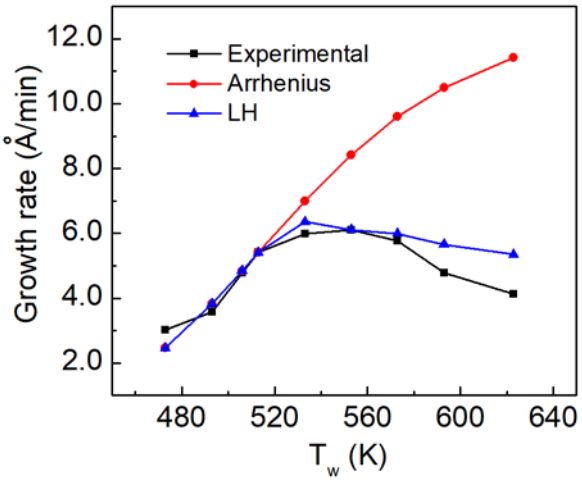

Figure 4.2 Deposition rate vs T_w as computed from the macro-scale model.

The two reaction kinetics, Arrhenius and LH are shown.

Table 4.1 The sticking coefficient $s_{[Cu(amd)]_2}$ and average, over the substrate area, mole fraction, $f_{[Cu(amd)]_2}$ of [Cu(amd)]$_2$ computed in the macro-scale and used in the kMC model.

$\boldsymbol{T_w}$ $\boldsymbol{[K]}$	473	493	506	513	533	553	573	593	623
$\boldsymbol{s_{[Cu(amd)]_2}}$	0.027	0.048	0.069	0.099	0.097	0.096	0.094	0.093	0.091
$< \boldsymbol{f_{[Cu(amd)]_2}} >$ $\boldsymbol{x10^5}$	5.94	5.12	4.55	3.96	3.98	3.99	3.99	4.01	4.02

growth rate (and the reaction rate for the particular case) is decreased. For T_w593 K and 623 K, $< f_{[Cu(amd)]_2} >$ is slightly increases but $s_{[Cu(amd)]_2}$ is decreased since in order to yield the decreased deposition rate in these T_w.

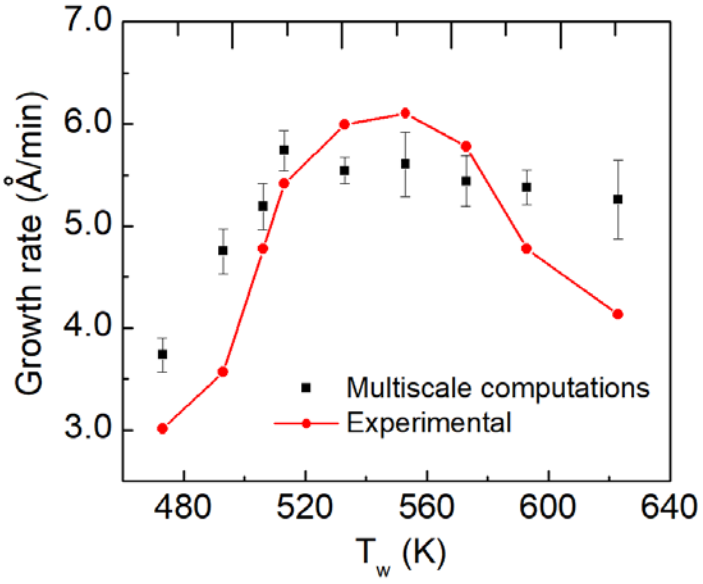

Figure 4.3 Growth rate vs T_w via multiscale computations. Information from the macro-scale of the CVD reactor is passed to the kMC model.

Using the data from Table 4.1 as input for the kMC model which explicitly takes into account inhibition effects from amd, described in Section 3.2, we predict the growth rates for every T_w shown in Fig. 4.3. In Fig. 4.3, the average growth rate over 10 kMC runs in a 300x300 lattice

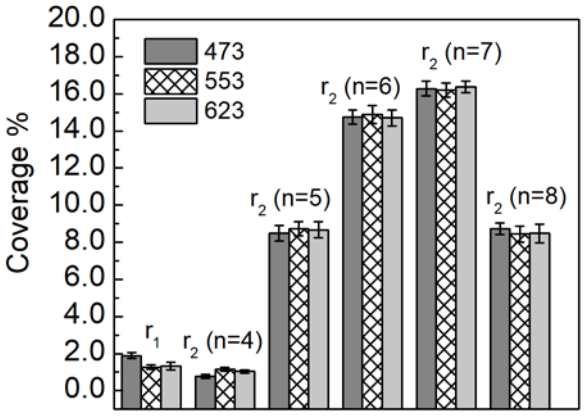

Figure 4.4 Surface coverage for T_w= 473 K, 553 K and 623 K.

is depicted. 10 s were adequate for the system to reach equilibrium. The growth rate is computed as the average height difference of the surface, $\Delta H_{Cu}/\Delta t$[102]where the lattice constant between two successive surfaces of Cu is 2.55 Å.

As it can be seen, the predicted growth rate is in satisfactory agreement with the experimental data up until 573 K. Above that T_w the results from the multiscale computations deviate from the experimental values. To better understand the results of Fig. 4.3, we construct the surface coverage i.e., the sites that are available for a process to perform, for 473 K, 553 K and 673 K. The results are shown in Fig. 4.4. When the system reaches equilibrium, in all cases almost half of the surface is idle i.e., half of the sites are blocked because cannot form quartets for the $[Cu(amd)]_2$ molecule to dissociate. The percentages of the idle surface in 473 K, 553 K and 673 K is 49.09 %, 49.33% and 49.41% respectively. Most of the rest of the surface is covered with $Cu_2(amd)$ and amd with coverage values of49.01 % (473 K), 49.40 % (553 K) and 49.27 % (623 K). The rest - 1.90% (473 K), 1.27 % (553 K) and 1.32 % (623 K) – is available for the dissociation of $[Cu(amd)]_2$. Note that $Cu_2(amd)$ and amd with less than 3 neighbors are instantly desorb. The maximum difference between the surfaces is observed in 473 K wherer_1 is ~33% higher compared to the higher temperature cases. Nevertheless,$s_{[Cu(amd)]_2}$ has the lowest value – see Table 4.1 – and for that, the lowest value of the growth is observed. As our model predicts, on the higher temperatures, the increase in T_s is not adequate to increases$_{[Cu(amd)]_2}$ sufficiently to saturate the surface and the inhibition effects to decrease the deposition rate. For that, most probable cause for the decrease of the growth rate in the high temperatures are the initiation of volumetric reactions in the bulk phase of the CVD reactor with a mechanism as reported in [10]. The initiation of the volumetric reactions causes the decrease of the mole fraction of the $[Cu(amd)]_2$ and consequently to the decrement of the deposition rate.

5. Conclusions

We developed a multiscale computations framework to explore the deposition of Cu from copper(I) N,N′-di-isopropylacetamidinate $[Cu(iPr–Me–amd)]_2$ or $[Cu(amd)]_2$ where amd = $CH(CH_3)_2NC(CH_3)NCH(CH_3)_2$. The multiscale model consists of a macro-scale model which describes the transport phenomena inside the CVD reactor based on the conservation equations (mass, momentum, energy and species mass fractions) and a kMC model which considers inhibition effects from the byproduct, namely H(amd) of the single surface reactor which leads to the deposition of Cu. The link point of the models is the boundary condition for the species equation i.e. the mass fractions and sticking coefficients computed in the macro-scale model is transferred to the kMC model. A single surface reaction is assumed in the macro-scale model according to previous experimental works.

Computations were performed for growth temperatures from 473 K to 623 K.The multiscale model satisfactory predicts the growth rate of Cu up until 573 K. Above this temperature, the computed growth rate deviates from the experimental data; the multiscale model predicts constant growth rate as the temperature increases while the experimental growth rate decreases. The latter is attributed to the initiation of volumetric reactions above 573 K which can reduce the mole fraction of the precursor leading to the further decrement of the growth rate. Concerning the kMC model, the desorption of H(amd) is assumed to be the limited step and is found to be barrierless (athermal) i.e. it does not depend on temperature and has small activation energy (0.09 eV). The latter, must be validated by DFT computations to validate our kMC model.

References

[1] N. Cheimarios, G. Kokkoris, and A. G. Boudouvis, "Multiscale Modeling in Chemical Vapor Deposition Processes: Models and Methodologies," *Arch. Comput. Methods Eng.*, vol. 28, no. 2, pp. 637–672, Mar. 2021, doi: 10.1007/s11831-019-09398-w.

[2] Z. Li, A. Rahtu, and R. G. Gordon, "Atomic Layer Deposition of Ultrathin Copper Metal Films from a Liquid Copper(I) Amidinate Precursor," *J. Electrochem. Soc.*, vol. 153, no. 11, p. C787, 2006, doi: 10.1149/1.2338632.

[3] D. Meulenbroeks, "Aluminum versus Copper Conductors: Application of Aluminum conductors in Bus Way systems for more sustainable Data Centers," Siemens, 2014.

[4] A. Pratt, "Overview of the Use of Copper Interconnects in the Semiconductor Industry," Advanced Energy Industries Inc., 2004.

[5] L. Wang and P. Clancy, "Kinetic Monte Carlo simulation of the growth of polycrystalline Cu films," *Surf. Sci.*, vol. 473, no. 1, pp. 25–38, Feb. 2001, doi: 10.1016/S0039-6028(00)00941-9.

[6] I. G. Aviziotis, N. Cheimarios, C. Vahlas, and A. G. Boudouvis, "Experimental and computational investigation of chemical vapor deposition of Cu from Cu amidinate," *Surf. Coat. Technol.*, vol. 230, pp. 273–278, 2013.

[7] A. Turgambaeva, N. Prud'homme, V. Krisyuk, and C. Vahlas, "Decomposition Schemes of Copper(I) N,N'-Diisopropylacetamidinate During Chemical Vapor Deposition of Copper," *J. Nanosci. Nanotechnol.*, vol. 11, no. 9, pp. 8198–8201, Sep. 2011, doi: 10.1166/jnn.2011.5099.

[8] D. Kim, R. H. Wentorf, and W. N. Gill, "Film Growth Kinetics of Chemical Vapor Deposition of Copper from Cu (HFA) 2," *J. Electrochem. Soc.*, vol. 140, no. 11, pp. 3267–3272, Nov. 1993, doi: 10.1149/1.2221021.

[9] J. Wang, R. B. Little, W. G. Lai, and G. L. Griffin, "Reactor transport effects in copper APCVD," *Copp.-Based Met. Interconnects Ultra-Large-Scale Integr. Appl.*, vol. 262, no. 1, pp. 31–38, Jun. 1995, doi: 10.1016/0040-6090(95)05832-X.

[10] R. Spencer, P. Gkinis, E. D. Koronaki, D. I. Gerogiorgis, S. P. A. Bordas, and A. G. Boudouvis, "Investigation of the chemical vapor deposition of Cu from copper amidinate through data driven efficient CFD modelling," *Comput. Chem. Eng.*, vol. 149, p. 107289, Jun. 2021, doi: 10.1016/j.compchemeng.2021.107289.

[11] N. Cheimarios, M. Kavousanakis, G. Kokkoris, and A. G. Boudouvis, "Beware of symmetry breaking and periodic flow regimes in axisymmetric CVD reactor setups," *Comput. Chem. Eng.*, vol. 124, pp. 124–132, May 2019, doi: 10.1016/j.compchemeng.2019.02.005.

[12] M. E. Coltrin, R. J. Kee, and G. H. Evans, "A Mathematical Model of the Fluid Mechanics and Gas-Phase Chemistry in a Rotating Disk Chemical Vapor Deposition Reactor," vol. 136, no. 3, 1989.

[13] M. E. Coltrin, R. J. Kee, and J. A. Miller, "A Mathematical Model of the Coupled Fluid Mechanics and Chemical Kinetics in a Chemical Vapor Deposition Reactor," *J. Electrochem. Soc.*, vol. 131, no. 2, pp. 425–434, 1984, doi: 10.1149/1.2115598.

[14] K. F. Jensen, "Transport phenomena and chemical reaction issues in OMVPE of compound semiconductors," *J. Cryst. Growth*, vol. 98, no. 1–2, pp. 148–166, 1989, doi: 10.1016/0022-0248(89)90195-4.

[15] K. F. Jensen and D. B. Graves, “Modeling and Analysis of Low Pressure CVD Reactors,” *J. Electrochem. Soc.*, vol. 130, no. 9, pp. 1950–1957, 1983, doi: 10.1149/1.2120129.
[16] C. R. Kleijn, “Computational modeling of transport phenomena and detailed chemistry in chemical vapor deposition – a benchmark solution,” *Thin Solid Films*, vol. 365, no. 2, pp. 294–306, Apr. 2000, doi: 10.1016/S0040-6090(99)01060-3.
[17] C. R. Kleijn, “A Mathematical Model of the Hydrodynamics and Gas-Phase Reactions in Silicon LPCVD in a Single-Wafer Reactor,” *J. Electrochem. Soc.*, vol. 138, no. 7, pp. 2190–2200, Jul. 1991, doi: 10.1149/1.2085948.
[18] C. R. Kleijn and C. J. Hoogendoorn, “A study of 2- and 3-D transport in horizontal chemical reactors phenomena,” vol. 46, no. 1, pp. 321–334, 1991.
[19] “Ansys/Fluent,” 2018. https://www.ansys.com/
[20] “Comsol,” 2018. https://www.comsol.com/
[21] T. C. Xenidou, N. Prud’homme, C. Vahlas, N. C. Markatos, and A. G. Boudouvis, “Reaction and Transport Interplay in Al MOCVD Investigated Through Experiments and Computational Fluid Dynamic Analysis,” *J. Electrochem. Soc.*, vol. 157, no. 12, pp. D633–D641, 2010, doi: 10.1149/1.3493617.
[22] T. C. Xenidou *et al.*, “An experimental and computational analysis of a MOCVD process for the growth of Al films using DMEAA,” *Surf. Coat. Technol.*, vol. 201, no. 22–23, pp. 8868–8872, 2007, doi: 10.1016/j.surfcoat.2007.04.080.
[23] A. I. Carim, N. A. Batara, A. Premkumar, H. A. Atwater, and N. S. Lewis, “Self-Optimizing Photoelectrochemical Growth of Nanopatterned Se-Te Films in Response to the Spectral Distribution of Incident Illumination,” *Nano Lett.*, vol. 15, no. 10, pp. 7071–7076, 2015, doi: 10.1021/acs.nanolett.5b03137.
[24] B. McKernan, K. E. S. Ford, R. O’Shaugnessy, and D. Wysocki, “Monte Carlo simulations of black hole mergers in AGN discs: Low χeff mergers and predictions for LIGO,” *Mon. Not. R. Astron. Soc.*, vol. 494, no. 1, pp. 1203–1216, May 2020, doi: 10.1093/mnras/staa740.
[25] I. Z. Emiris and V. Fisikopoulos, “Practical Polytope Volume Approximation,” *ACM Trans Math Softw*, vol. 44, no. 4, 2018, doi: 10.1145/3194656.
[26] H. Cansizoglu, M. F. Cansizoglu, and T. Karabacak, “Effect of shell coating technique on carrier collection properties of core/shell nanostructures,” 2015. doi: 10.1109/PVSC.2015.7355813.
[27] J. Yang, Y. Zhou, and B. Pu, “Three-dimensional ES barrier promotes the steps formation,” vol. 783. Trans Tech Publications Ltd, School of Materials and Energy, University of Electronic Science and Technology of China, Chengdu, 610054, China, pp. 115–119, 2018. doi: 10.4028/www.scientific.net/KEM.783.115.
[28] Y. Ding, Y. Zhang, Y. M. Ren, G. Orkoulas, and P. D. Christofides, “Machine learning-based modeling and operation for ALD of SiO2 thin-films using data from a multiscale CFD simulation,” *Chem. Eng. Res. Des.*, vol. 151, pp. 131–145, 2019, doi: 10.1016/j.cherd.2019.09.005.
[29] H. Jiang and Z. Hou, “Large-scale epitaxial growth kinetics of graphene: A kinetic Monte Carlo study,” *J. Chem. Phys.*, vol. 143, no. 8, 2015, doi: 10.1063/1.4929471.
[30] P. Poodt, A. Mameli, J. Schulpen, W. M. M. Kessels, and F. Roozeboom, “Effect of reactor pressure on the conformal coating inside porous substrates by atomic layer deposition,” *J. Vac. Sci. Technol. Vac. Surf. Films*, vol. 35, no. 2, 2017, doi: 10.1116/1.4973350.

[31] H. Cansizoglu, M. Yurukcu, M. F. Cansizoglu, and T. Karabacak, “Investigation of physical vapor deposition techniques of conformal shell coating for core/shell structures by Monte Carlo simulations,” *Thin Solid Films*, vol. 583, no. 1, pp. 122–128, 2015, doi: 10.1016/j.tsf.2015.03.071.
[32] F. Du and H. Huang, “A theory of growing crystalline nanorods – Mode I,” *Surf. Sci.*, vol. 674, pp. 18–24, 2018, doi: 10.1016/j.susc.2018.03.016.
[33] M. Yurukcu, H. Cansizoglu, M. F. Cansizoglu, and T. Karabacak, “Conformality of PVD shell layers on vertical arrays of rods with different aspect ratios investigated by Monte Carlo simulations,” in *MRS Advances*, 2017, vol. 2, no. 8, pp. 465–470. doi: 10.1557/adv.2017.158.
[34] S. Chen *et al.*, “An all-atom kinetic Monte Carlo model for chemical vapor deposition growth of graphene on Cu(1 1 1) substrate,” *J. Phys. Condens. Matter*, vol. 32, no. 15, 2020, doi: 10.1088/1361-648X/ab62bf.
[35] S. Chen *et al.*, “A kinetic Monte Carlo model for the growth and etching of graphene during chemical vapor deposition,” *Carbon*, vol. 146, pp. 399–405, 2019, doi: 10.1016/j.carbon.2019.02.016.
[36] S. Chen *et al.*, “Unveiling the competitive role of etching in graphene growth during chemical vapor deposition,” *2D Mater.*, vol. 6, no. 1, 2019, doi: 10.1088/2053-1583/aaf59c.
[37] G. Enstone, P. Brommer, D. Quigley, and G. R. Bell, “Enhancement of island size by dynamic substrate disorder in simulations of graphene growth,” *Phys Chem Chem Phys*, vol. 18, no. 22, pp. 15102–15109, 2016, doi: 10.1039/C6CP00788K.
[38] P. Gaillard, A. L. Schoenhalz, P. Moskovkin, S. Lucas, and L. Henrard, “Growth of nitrogen-doped graphene on copper: Multiscale simulations,” *Surf. Sci.*, vol. 644, pp. 102–108, 2016, doi: 10.1016/j.susc.2015.08.038.
[39] P. Gaillard, T. Chanier, L. Henrard, P. Moskovkin, and S. Lucas, “Multiscale simulations of the early stages of the growth of graphene on copper,” *Surf. Sci.*, vol. 637–638, pp. 11–18, 2015, doi: 10.1016/j.susc.2015.02.014.
[40] F. Göltl, E. A. Murray, B. W. J. Chen, R. M. Jacobberger, M. S. Arnold, and M. Mavrikakis, “Exploring driving forces for length growth in graphene nanoribbons during chemical vapor deposition of hydrocarbons on Ge(0 0 1) via kinetic Monte Carlo simulations,” *Appl. Surf. Sci.*, vol. 527, 2020, doi: 10.1016/j.apsusc.2020.146784.
[41] S. Chen *et al.*, “Origin of ultrafast growth of monolayer WSe2 via chemical vapor deposition,” *Npj Comput. Mater.*, vol. 5, no. 1, p. 28, Dec. 2019, doi: 10.1038/s41524-019-0167-2.
[42] A. Govind Rajan, J. H. Warner, D. Blankschtein, and M. S. Strano, “Generalized Mechanistic Model for the Chemical Vapor Deposition of 2D Transition Metal Dichalcogenide Monolayers,” *ACS Nano*, vol. 10, no. 4, pp. 4330–4344, 2016, doi: 10.1021/acsnano.5b07916.
[43] X. Li *et al.*, “Mo Concentration Controls the Morphological Transitions from Dendritic to Semicompact, and to Compact Growth of Monolayer Crystalline MoS2 on Various Substrates,” *ACS Appl. Mater. Interfaces*, vol. 11, no. 45, pp. 42751–42759, 2019, doi: 10.1021/acsami.9b14577.
[44] Y. Nie *et al.*, “First principles kinetic Monte Carlo study on the growth patterns of WSe<inf>2</inf> monolayer,” *2D Mater.*, vol. 3, no. 2, 2016, doi: 10.1088/2053-1583/3/2/025029.

[45] L. Wu, W. Yang, and G. Wang, “Mechanism of substrate-induced anisotropic growth of monolayer WS2 by kinetic Monte Carlo simulations,” *Npj 2D Mater. Appl.*, vol. 3, no. 1, 2019, doi: 10.1038/s41699-019-0088-4.

[46] R. Yue *et al.*, “Nucleation and growth of WSe2: enabling large grain transition metal dichalcogenides,” *2D Mater.*, vol. 4, no. 4, 2017, doi: 10.1088/2053-1583/aa8ab5.

[47] B. A. Reshi, M. J. Kartha, A. Misra, and R. Varma, “Investigation of diamond deposition on the diamond, silicon and quartz substrates by microwave plasma chemical vapor deposition and Monte Carlo simulations,” *Mater. Res. Express*, vol. 6, no. 9, 2019, doi: 10.1088/2053-1591/ab2e8e.

[48] J. An, X. Dai, W. Wu, R. Guo, and L. Feng, “Kinetic Monte Carlo Simulation of the Growth of AlN Films by Metal Organic Chemical Vapor Deposition,” *Phys. Status Solidi B Basic Res.*, vol. 256, no. 12, 2019, doi: 10.1002/pssb.201900114.

[49] P. K. Saxena, P. Srivastava, and R. Trigunayat, “An innovative approach for controlled epitaxial growth of GaAs in real MOCVD reactor environment,” *J. Alloys Compd.*, vol. 809, 2019, doi: 10.1016/j.jallcom.2019.151752.

[50] O. Babahani, S. Hadjadj, F. Khelfaoui, H. O. Kebaili, and S. Lemkeddem, “Monte Carlo Simulation of Chemical Reactions in Plasma Enhanced Chemical Vapor Deposition: from Microscopic View to Macroscopic Results,” *Silicon*, vol. 11, no. 3, pp. 1267–1274, 2019, doi: 10.1007/s12633-018-9916-y.

[51] Y. Zhang, H. Wang, Y. Gou, and S. Jiang, “Evolution of medium-range order and surface compositions by mechanism-driven model with realistic network,” *Appl. Surf. Sci.*, vol. 464, pp. 321–327, 2019, doi: 10.1016/j.apsusc.2018.09.090.

[52] N. Pittman and T.-M. Lu, “Growth front smoothing effects in extremely high pressure vapor deposition,” *Sci. Rep.*, vol. 10, no. 1, 2020, doi: 10.1038/s41598-020-69269-4.

[53] V. Cremers, F. Geenen, C. Detavernier, and J. Dendooven, “Monte Carlo simulations of atomic layer deposition on 3D large surface area structures: Required precursor exposure for pillar- versus hole-type structures,” *J. Vac. Sci. Technol. Vac. Surf. Films*, vol. 35, no. 1, 2017, doi: 10.1116/1.4968201.

[54] T. Muneshwar, G. Shoute, D. Barlage, and K. Cadien, “Parasitic Surface Reactions in High-Aspect Ratio Via Filling using ALD: A Stochastic Kinetic Model,” 2019, vol. 2018-Decem, p. 40.2.1-40.2.4. doi: 10.1109/IEDM.2018.8614584.

[55] M. C. Schwille *et al.*, “Experimental and simulation approach for process optimization of atomic layer deposited thin films in high aspect ratio 3D structures,” *J. Vac. Sci. Technol. Vac. Surf. Films*, vol. 35, no. 1, 2017, doi: 10.1116/1.4971196.

[56] M. C. Schwille, J. Barth, T. Schössler, F. Schön, J. W. Bartha, and M. Oettel, “Simulation approach of atomic layer deposition in large 3D structures,” *Model. Simul. Mater. Sci. Eng.*, vol. 25, no. 3, 2017, doi: 10.1088/1361-651X/aa5f9d.

[57] N. Sitapure, H. Lee, F. Ospina-Acevedo, P. B. Balbuena, S. Hwang, and J. S.-I. Kwon, “A computational approach to characterize formation of a passivation layer in lithium metal anodes,” *AIChE J.*, 2020, doi: 10.1002/aic.17073.

[58] B. S. Vishnugopi, F. Hao, A. Verma, and P. P. Mukherjee, “Surface diffusion manifestation in electrodeposition of metal anodes,” *Phys. Chem. Chem. Phys.*, vol. 22, no. 20, pp. 11286–11295, 2020, doi: 10.1039/d0cp01352h.

[59] D. A. Spade, “Chapter 1 - Markov chain Monte Carlo methods: Theory and practice,” in *Principles and Methods for Data Science*, vol. 43, A. S. R. Srinivasa Rao and C. R. B. T.-H. of S. Rao, Eds. Elsevier, 2020, pp. 1–66. doi: https://doi.org/10.1016/bs.host.2019.06.001.
[60] N. Metropolis, A. W. Rosenbluth, M. N. Rosenbluth, A. H. Teller, and E. Teller, “Equation of State Calculations by Fast Computing Machines,” *J. Chem. Phys.*, vol. 21, no. 6, pp. 1087–1092, Jun. 1953, doi: 10.1063/1.1699114.
[61] A. B. Bortz, M. H. Kalos, and J. L. Lebowitz, “A new algorithm for Monte Carlo simulation of Ising spin systems,” *J. Comput. Phys.*, vol. 17, no. 1, pp. 10–18, 1975, doi: https://doi.org/10.1016/0021-9991(75)90060-1.
[62] A. F. Voter, “Introduction to the kinetic Monte Carlo Method - Radiation Effects in Solids,” 2007, pp. 1–23.
[63] J. P. Balbuena and I. Martin-Bragado, “Lattice kinetic Monte Carlo simulation of epitaxial growth of silicon thin films in H<inf>2</inf>/SiH<inf>4</inf> chemical vapor deposition systems,” *Thin Solid Films*, vol. 634, pp. 121–133, 2017, doi: 10.1016/j.tsf.2017.05.013.
[64] S. D. Collins, A. Chatterjee, and D. G. Vlachos, “Coarse-grained kinetic Monte Carlo models: Complex lattices, multicomponent systems, and homogenization at the stochastic level,” *J. Chem. Phys.*, vol. 129, no. 18, p. 184101, Nov. 2008, doi: 10.1063/1.3005225.
[65] Z. Zheng, R. M. Stephens, R. D. Braatz, R. C. Alkire, and L. R. Petzold, “A hybrid multiscale kinetic Monte Carlo method for simulation of copper electrodeposition,” *J. Comput. Phys.*, vol. 227, no. 10, pp. 5184–5199, 2008, doi: https://doi.org/10.1016/j.jcp.2008.01.056.
[66] M. Trochet, N. Mousseau, L. K. Béland, and G. Henkelman, “Off-Lattice Kinetic Monte Carlo Methods BT - Handbook of Materials Modeling: Methods: Theory and Modeling,” W. Andreoni and S. Yip, Eds. Cham: Springer International Publishing, 2020, pp. 715–743. doi: 10.1007/978-3-319-44677-6_29.
[67] J. Guerrero-Sánchez, N. Takeuchi, and F. Zaera, “Density Functional Theory Study of the Surface Adsorption and Dissociation of Copper(I) Acetamidinates on Cu(110) Surfaces,” *J. Phys. Chem. C*, vol. 123, no. 7, pp. 4341–4348, Feb. 2019, doi: 10.1021/acs.jpcc.8b12131.
[68] R. Lam and D. Vlachos, “Multiscale model for epitaxial growth of films: Growth mode transition,” *Phys. Rev. B*, vol. 64, no. 3, pp. 035401–035401, Jun. 2001, doi: 10.1103/PhysRevB.64.035401.
[69] Z. A. Piskulich, O. O. Mesele, and W. H. Thompson, “Activation Energies and Beyond,” *J. Phys. Chem. A*, vol. 123, no. 33, pp. 7185–7194, Aug. 2019, doi: 10.1021/acs.jpca.9b03967.
[70] E. I. Estrin, “Athermal processes in solids,” *Bull. Russ. Acad. Sci. Phys.*, vol. 71, no. 12, pp. 1649–1655, Dec. 2007, doi: 10.3103/S1062873807120015.
[71] C. Filippi, S. B. Healy, P. Kratzer, E. Pehlke, and M. Scheffler, “Quantum Monte Carlo Calculations of ${\mathrm{H}}_{2}$ Dissociation on Si(001),” *Phys. Rev. Lett.*, vol. 89, no. 16, p. 166102, Sep. 2002, doi: 10.1103/PhysRevLett.89.166102.
[72] W. Brenig, H. J. Kreuzer, and S. H. Payne, “Reactions of hydrogen on silicon: Kinetics and dynamics,” *Phys. Rev. B*, vol. 67, no. 20, p. 205419, May 2003, doi: 10.1103/PhysRevB.67.205419.
[73] C. Zhou *et al.*, “Hydrogen dissociative chemisorption and desorption on saturated subnano palladium clusters (Pdn, n = 2–9),” *Phys. Chem. Chem. Phys.*, vol. 10, no. 35, pp. 5445–5451, 2008, doi: 10.1039/B804877K.
[74] *SPPARKS*. 2008. [Online]. Available: https://spparks.github.io/

[75] *ZACROS*. 2013. [Online]. Available: https://stamatakislab.org/software.html
[76] M. Leetmaa and N. V. Skorodumova, "KMCLib: A general framework for lattice kinetic Monte Carlo (KMC) simulations," *Comput. Phys. Commun.*, vol. 185, no. 9, pp. 2340–2349, Sep. 2014, doi: 10.1016/j.cpc.2014.04.017.
[77] *NASCAM*. 2016. [Online]. Available: https://www.unamur.be/sciences/physique/ur/larn/logiciels/nascam
[78] M. Andersen, C. Panosetti, and K. Reuter, "A Practical Guide to Surface Kinetic Monte Carlo Simulations," *Front. Chem.*, vol. 7, p. 202, 2019, doi: 10.3389/fchem.2019.00202.
[79] D. J. Srolovitz, D. S. Dandy, J. E. Butler, and C. C. Battaile, "The integrated multiscale modeling of diamond chemical vapor deposition," *Jom*, vol. 49, no. 9, pp. 42–47, Sep. 1997, doi: 10.1007/BF02914350.
[80] D. G. Vlachos, "Multiscale Integration Hybrid Algorithms for Homogeneous-Heterogeneous Reactors," *Aiche J.*, vol. 43, no. 11, pp. 3031–3041, 1997.
[81] D. G. Vlachos, "The role of macroscopic transport phenomena in film microstructure during epitaxial growth," *Appl. Phys. Lett.*, vol. 74, no. 19, pp. 2797–2797, 1999, doi: 10.1063/1.124017.
[82] S. Raimondeau and D. G. Vlachos, "Low-Dimensional Approximations of Multiscale Epitaxial Growth Models for Microstructure Control of Materials," *J Comput Phys*, vol. 160, no. 2, pp. 564–576, May 2000, doi: 10.1006/jcph.2000.6473.
[83] M. Masi, V. Bertani, C. Cavallotti, and S. Carrà, "Towards a multiscale approach to the growth of silicon films by chemical vapor deposition," *Mater. Chem. Phys.*, vol. 66, no. 2–3, pp. 229–235, Oct. 2000, doi: 10.1016/S0254-0584(00)00323-0.
[84] M. Grujicic and S. G. Lai, "Multi-length scale modeling of chemical vapor deposition of titanium nitride coatings," vol. 6, pp. 2937–2953, 2001.
[85] A. Dollet, S. de Persis, M. Pons, and M. Matecki, "Simulation of SiC deposition from SiH4/C3H8/Ar/H2 mixtures in a cold-wall CVD reactor," *Surf. Coat. Technol.*, vol. 177–178, pp. 382–388, Jan. 2004, doi: 10.1016/j.surfcoat.2003.09.032.
[86] C. Cavallotti, M. Di Stanislao, D. Moscatelli, and A. Veneroni, "Materials computation towards technological impact: The multiscale approach to thin films deposition," *Electrochimica Acta*, vol. 50, no. 23, pp. 4566–4575, 2005, doi: 10.1016/j.electacta.2004.10.092.
[87] C. Cavallotti, E. Pantano, A. Veneroni, and M. Masi, "Multiscale simulation of silicon film growth," *Cryst. Res. Technol.*, vol. 40, no. 10–11, pp. 958–963, 2005.
[88] A. Barbato, A. Fiorucci, M. Rondanini, and C. Cavallotti, "Multiscale investigation of the influence of surface morphology on thin film CVD," *Surf. Coat. Technol.*, vol. 201, no. 22–23, pp. 8884–8887, 2007, doi: 10.1016/j.surfcoat.2007.04.071.
[89] A. Barbato and C. Cavallotti, "Challenges of introducing quantitative elementary reactions in multiscale models of thin film deposition," *Phys. Status Solidi B Basic Res.*, vol. 247, no. 9, pp. 2127–2146, Sep. 2010, doi: 10.1002/pssb.200945454.
[90] M. Masi, A. Fiorucci, M. Camarda, A. La Magna, and F. La Via, "Multiscale simulation for epitaxial silicon carbide growth by chlorides route," *Thin Solid Films*, vol. 518, no. 6, pp. S6–S11, Jan. 2010, doi: 10.1016/j.tsf.2009.10.045.
[91] N. Cheimarios, S. Garnelis, G. Kokkoris, and A. G. Boudouvis, "Linking the Operating Parameters of Chemical Vapor Deposition Reactors with Film Conformality and Surface

Nano-Morphology," *J. Nanosci. Nanotechnol.*, vol. 11, no. 9, pp. 8132–8137, 2011, doi: 10.1166/jnn.2011.5076.

[92] I. G. Aviziotis, N. Cheimarios, T. Duguet, C. Vahlas, and A. G. Boudouvis, "Multiscale modeling and experimental analysis of chemical vapor deposited aluminum films: Linking reactor operating conditions with roughness evolution," *Chem. Eng. Sci.*, vol. 155, 2016, doi: 10.1016/j.ces.2016.08.039.

[93] I. G. Aviziotis, T. Duguet, C. Vahlas, and A. G. Boudouvis, "Combined Macro/Nanoscale Investigation of the Chemical Vapor Deposition of Fe from Fe(CO)5," *Adv. Mater. Interfaces*, vol. 4, no. 18, p. 1601185, Sep. 2017, doi: https://doi.org/10.1002/admi.201601185.

[94] P. Wang, R. Mücke, W. He, G. Mauer, and R. Vaßen, "Fluid dynamics and modelling of plasma jet in PS-PVD process and Monte Carlo simulations of PS-PVD columns," 2016, vol. 1, pp. 190–195.

[95] Y. Zhang, Y. Ding, and P. D. Christofides, "Integrating feedback control and run-to-run control in multi-wafer thermal atomic layer deposition of thin films," *Processes*, vol. 8, no. 1, 2020, doi: 10.3390/pr8010018.

[96] Y. Ding, Y. Zhang, G. Orkoulas, and P. D. Christofides, "Microscopic modeling and optimal operation of plasma enhanced atomic layer deposition," *Chem. Eng. Res. Des.*, vol. 159, pp. 439–454, 2020, doi: 10.1016/j.cherd.2020.05.014.

[97] Y. Zhang, Y. Ding, and P. D. Christofides, "Multiscale computational fluid dynamics modeling and reactor design of plasma-enhanced atomic layer deposition," *Comput. Chem. Eng.*, vol. 142, 2020, doi: 10.1016/j.compchemeng.2020.107066.

[98] Y. Zhang, Y. Ding, Z. Wu, and P. D. Christofides, "Run-to-run control of thermal atomic layer deposition," in *2020 28th Mediterranean Conference on Control and Automation, MED 2020*, 2020, pp. 1080–1086. doi: 10.1109/MED48518.2020.9183059.

[99] Y. Ding, Y. Zhang, K. Kim, A. Tran, Z. Wu, and P. D. Christofides, "Microscopic modeling and optimal operation of thermal atomic layer deposition," *Chem. Eng. Res. Des.*, vol. 145, pp. 159–172, 2019, doi: 10.1016/j.cherd.2019.03.004.

[100] N. Cheimarios, G. Kokkoris, and A. G. Boudouvis, "Multiscale modeling in chemical vapor deposition processes: Coupling reactor scale with feature scale computations," *Chem. Eng. Sci.*, vol. 65, no. 17, pp. 5018–5028, 2010, doi: 10.1016/j.ces.2010.06.004.

[101] N. Cheimarios, G. Kokkoris, and A. G. Boudouvis, "A multi-parallel multiscale computational framework for chemical vapor deposition processes," *J. Comput. Sci.*, vol. 15, 2016, doi: 10.1016/j.jocs.2015.08.011.

[102] K. Fu and Y. Fu, "Kinetic Monte Carlo study of metal organic chemical vapor deposition growth mechanism of GaSb quantum dots," *Appl. Phys. Lett.*, vol. 93, no. 10, p. 101906, Sep. 2008, doi: 10.1063/1.2981515.